Journal of Power Sources 195 (2010) 4051–4058

Contents lists available at ScienceDirect

Journal of Power Sources

journal homepage: www.elsevier.com/locate/jpowsour

Evaluation of raw coals as fuels for direct carbon fuel cells

Xiang Li[a], Zhonghua Zhu[a,*], Roland De Marco[b], John Bradley[a], Andrew Dicks[a]

[a] School of Chemical Engineering, University of Queensland, St Lucia, Brisbane, QLD 4072, Australia
[b] Nanochemistry Research Institute, Department of Chemistry, Curtin University of Technology, Perth, Western Australia 6845, Australia

ARTICLE INFO

Article history:
Received 9 October 2009
Received in revised form
10 December 2009
Accepted 8 January 2010
Available online 1 February 2010

Keywords:
Direct carbon fuel cell
Coal
Electrochemical reactivity
Impurities

ABSTRACT

As a promising high-temperature fuel cell, the direct carbon fuel cell (DCFC) has a much higher efficiency and lower emissions compared with conventional coal-fired power plants. In the present DCFC system, four Australian coals from Central Queensland are successfully tested at 600–800 °C. The electrochemical performances of these coals are highly dependent on their intrinsic properties, such as chemical composition, surface area, concentrations of oxygen-containing surface functional groups and the nature of mineral matter in their ashes. Impurities such as Al_2O_3 and SiO_2 lead to an inhibitive effect during the anodic reaction in the DCFC, while CaO, MgO and Fe_2O_3 exhibit a catalytic effect on the electrochemical oxidation of carbon.

1. Introduction

Coal is the most abundant and economic fossil resource on the earth and presently accounts for 25% of the world's primary energy consumption, and is forecast to account for 28% of the world's increased primary energy consumption by 2030 [1]. Most energy reserves of coal, however, remain underused and copious amounts of greenhouse gases are produced by conventional coal-fired plants. In this regard, the direct carbon fuel cell (DCFC) would be a more effective means of electricity generation due to its high energy-conversion efficiency with low pollution. As a high-temperature fuel cell, the DCFC has the significant thermodynamic advantage of a near zero entropy change at high temperature, which means the theoretical electrochemical efficiency of the DCFC ($\Delta G/\Delta H$) is almost 100% [2–5]. Even under practical conditions, an approximate 80% efficiency can be reached in the DCFC system. Moreover, the activities (chemical potentials) of both reactant carbon and the product carbon dioxide are fixed and thereby result in a stable carbon anode potential during practical operation [2]. Last but not least, the DCFC has lower emissions compared with conventional power plants. In principle, the off-gas can be pure carbon dioxide, which can be directly collected for industrial use or sequestration [2,3].

Until now, there have been different attempts to convert carbon materials directly into electricity in the DCFC with various electrolytes, such as molten carbonates [2,6,7], molten hydroxides [5,8,9] and yttria-stabilized zirconia (YSZ)-based solid electrolytes [10–13]. One of the latest developments in DCFC technology is to utilize highly-reactive carbon particulates dispersed in a molten carbonate electrolyte, which flows between the anode and cathode at high temperature [2,6,7]. The anode and cathode reactions may be expressed by Eqs. (1) and (2), respectively while the overall reaction is given by Eq. (3) [2,6].

$$\text{Anode reaction}: \quad C + 2CO_3^{2-} \rightarrow 3CO_2 + 4e^- \tag{1}$$

$$\text{Cathode reaction}: \quad O_2 + 2CO_2 + 4e^- \rightarrow 2CO_3^{2-} \tag{2}$$

$$\text{Overall reaction}: \quad C + O_2 \rightarrow CO_2 \tag{3}$$

The anode potential is given by:

$$E_{\text{cell}} = E^\circ - \left(\frac{RT}{4F}\right) \ln[P^3_{CO_2}(w)] + \left(\frac{RT}{4F}\right) \ln[P^2_{CO_2}(r)\, P_{O_2}(r)] \tag{4}$$

where: E° is the anode potential at standard condition; R is the universal gas constant; T is the cell temperature (K); $P_{CO_2}(w)$ is the CO_2 partial pressure to total pressure at the working electrode; $P_{CO_2}(r)$ and $P_{O_2}(r)$ are the partial pressures of CO_2 and O_2 to total pressure at the reference electrode, respectively.

As the most prospective fuel for DCFCs, coal is a complex chemically and physically heterogeneous conglomerate, that contains various organic and inorganic materials [14]. Various impurities in coals have side-effects on the anodic electrochemical reaction and the lifetime of the DCFC, as suggested by other researchers [2,3,6,7,15]. Weaver and Nanis [7] were the first to report that the addition of 10 wt.% fly ash into a DCFC did not change the potential–current (or V–i) curves measurably. Vutetakis et al. [6],

* Corresponding author. Tel.: +61 7 3365 3528; fax: +61 7 3365 4199.
E-mail address: z.zhu@uq.edu.au (Z. Zhu).

0378-7753/$ – see front matter © 2010 Elsevier B.V. All rights reserved.
doi:10.1016/j.jpowsour.2010.01.048

however, studied the effect of various mineral impurities in their DCFC, and observed a sharp drop in current at high overpotentials that might be due to passivation of electrodes by dissolved coal ashes. Cherapy et al. [2] recently tested petroleum cokes containing 2.5–6 wt.% sulfur in a DCFC and reported that sulfidic corrosion at the anode degraded cell performance over time. Unfortunately, these authors did not report the influence of other impurities in the tested cokes on DCFC performance to ascertain the level of purity needed for the successful use of coal.

In a recent paper by the present authors [16], a Queensland Germancreek (GK) coal was tested as a fuel in a DCFC system. The GK coal was treated by different acids and gases. It was found that nitric acid can not only improve the electrochemical activity of coal by adding more CO_2-yielding surface groups, but may also remove ash and thereby protect the electrolyte and electrodes. In this study, three other Queensland coals called Blackwater (BW), Kinston (KT) and Newland (NL) are compared with GK in a DCFC system at 600–800 °C. Based on a comprehensive characterization of the microstructure along with physical and chemical properties, the electrochemical reactivities of the coals are examined. In addition, a comparative study is conducted into the influence of different impurities in the coal ashes on the electrochemical performance of the DCFC.

2. Experimental

2.1. Characterization of coal samples

Four raw coals from different parts of central Queensland, namely, Germancreek (GK), Blackwater (BW), Kinston (KT) and Newland (NL), were ground and sieved to 1–2 mm particle sizes. The weight losses of the coals were investigated by thermogravimetric analysis (Shimadzu TGA-50) as recommended in Ref. [17]. The air-dried coal samples were heated in N_2 (80 ml min^{-1}) from room temperature to 110 °C (20 °C min^{-1}) until a constant weight was reached after holding at 110 °C for 20 min, at which point the weight loss due to moisture removal was observed. The samples, still held in flowing N_2, were subsequently heated from 110 to 950 °C (50 °C min^{-1}) and maintained at 950 °C for 30 min, during which a second weight loss corresponding to volatile matter was observed. Subsequently, the purge gas was switched from N_2 to air (80 ml min^{-1}), and a rapid weight loss occurred on account of the burning off of fixed carbon. The remaining weight was the amount of ash.

The mineral matter in the raw coals was first separated from the coals by oxidation at 700 °C in a tube furnace under an air atmosphere for 2 h. The ash composition was determined by means of inductively-coupled plasma optical emission spectrometry (ICPOES). A 0.5 g sample of coal ash sample was weighed into a Teflon vessel, to which an acid mixture containing 10 ml of water, 5 ml of HNO_3 (37%), 4 ml of HF (50%) and 2 ml of HCl (35%) was added. After predigestion sample for 16 h, the sample was subjected to microwave-assisted acid digestion in a digestor (CEM MDS2000) at 68% power for 20 min. The digested sample was made up to a volume of 50 ml with saturated boric acid to react with excess HF. Finally, the sample was analysed by a Varian Vista Pro ICPOES instrument that operated at 1200 W forward power.

X-ray diffraction (XRD) characterization of coal samples was performed on a Rigaku Miniflex X-ray diffractometer (40 kV, 30 mA) with Co Kα (λ = 0.17902 nm) radiation at a scanning rate of 2° min^{-1} in the 2θ range from 10° to 90°. The average size of carbon crystallites was calculated from the Debye–Scherrer equation:

$$L = \frac{K\lambda}{\beta \cos\theta} \quad (5)$$

where: λ is the wavelength of the X-rays; θ is the diffraction angle; K is the shape factor; β is the peak width at half-maximum intensity. The values of K = 0.89 and 1.84 were used in the determination of the crystallite size parameters Lc and La, respectively [18]. The layer dimension perpendicular to the basal plane, Lc, is obtained from the (0 0 2) reflection. The layer dimension parallel to the basal plane, La, is calculated from the (1 0 0) reflection.

Nitrogen adsorption experiments were carried out in a Quadrasorb adsorption analyser (Quantachrome, USA) at −196 °C. The specific surface areas (S_{BET}) of the carbon samples were calculated by the multiple-point Brunauer–Emmett–Teller (BET) method in the relative pressure range P/P_o = 0.05–0.25. The total pore volume (V_{total}) was derived from the amount of nitrogen adsorbed at a relative pressure of P/P_o = 0.99. The average pore diameters (D_{pore}) of carbons were calculated using commercial software (QuadraWin V2.0), which applied the Barrett–Joyner–Hallenda (BJH) method. Prior to the nitrogen adsorption measurements, all samples were degassed at 200 °C overnight.

Carbon dioxide adsorption data were obtained by means of an Autosorb instrument (Quantachrome, USA) at 0 °C. The micropore volume (V_{micro}), surface area (S_{micro}) and average pore size (D_{micro}) of samples were calculated using commercial software (QuadraWin V2.0), which applied the Dubinin–Radushkevich (DR) method. Prior to the CO_2 adsorption experiments, all samples were degassed at 110 °C overnight.

X-ray photoelectron spectroscopy (XPS) measurements were performed on a Kratos Axis Ultra XPS system that incorporated a 165 mm hemispherical electron energy analyser. XPS spectra were obtained using a monochromatic Al Kα X-ray (1486.6 eV) source operated at 150 W (15 kV, 10 mA). Survey scans were performed over a 1200 eV binding energy range at a pass energy of 160 eV using a 1.0 eV step and a dwell time of 100 ms. The vacuum pressure was maintained at about 10^{-9} Torr during all experiments.

Temperature-programmed desorption (TPD) experiments were carried out in a vertical tube furnace with argon (80 ml min^{-1}) as the carrier gas. Each time, 0.5 g of sample was placed in a quartz tube reactor, heated to 110 °C and held for 60 min before subsequent ramping at 5 °C min^{-1} to 900 °C. The gases evolved were analysed with a gas chromatograph (Shimadzu GC-17A) that was equipped with a thermal conductivity detector and a Carbosphere column [19].

2.2. Evaluation of coals in DCFC

Fig. 1 shows a schematic diagram of the DCFC used in the work. The cell employed a molten carbonate electrolyte under stirred conditions to improve mass transportation at the electrode surface. The cell design reported herein focused on the electrochemistry of the anode reaction; the cathode reactions at the counter electrode were ignored. The design details of the DCFC system have been reported elsewhere [6,16,20–22]. Prior to each experiment, 250 g of dry ternary carbonate powder (32 wt.%Li_2CO_3–34 wt.%Na_2CO_3–34 wt.%K_2CO_3) was mixed with 12.5 g of the coal (viz., 5 wt.% carbon fuel in the carbonate electrolyte). The gold parts of the three different electrodes were washed by nitrohydrochloric acid for 10 s before rinsing with distilled water and then with acetone. After the fuel cell was assembled and sealed gastight, it was heated by a crucible furnace (Lindberg Blue/M) at a rate of 3 °C min^{-1}. During the heat-up stage, argon (150 ml min^{-1}) was purged into the working electrode (WE) compartment and CO_2 (50 ml min^{-1}) was purged into the counter electrode (CE) and reference electrode (RE) compartments. Once the required operating temperature was reached, the argon and CO_2 purge rates were decreased to 70 and 15 ml min^{-1}, respectively. At the same time, air (35 ml min^{-1}) was introduced into

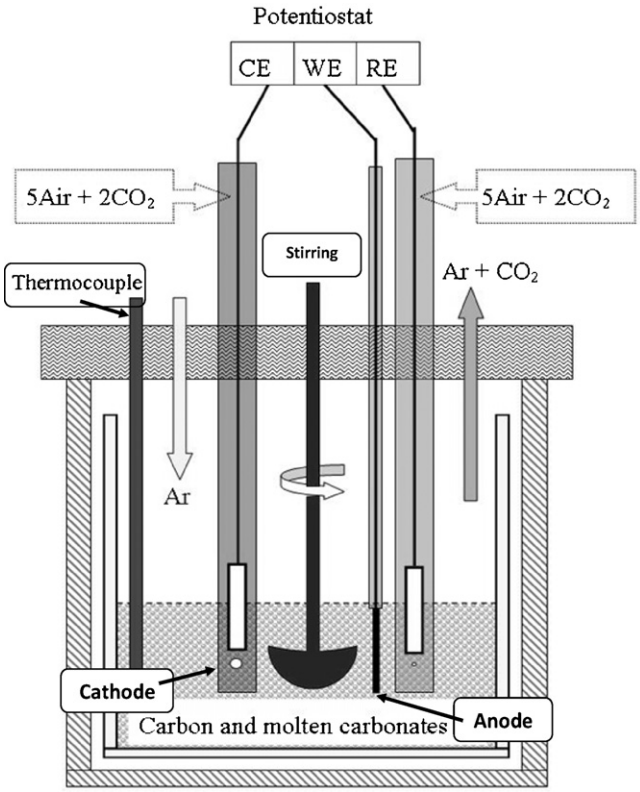

Fig. 1. Schematic diagram of DCFC [note that ingression of carbon particles to cathode (CE) is prevented by a hole size of 1 mm on sheath of CE that is smaller than particle sizes of coals (>1 mm)].

the CE and RE compartments. Finally, the carbon anode half-cell measurements were performed with a potentiostat (Autolab PGSTAT302), using the GPES software package (Version 4.9). For linear sweep voltammetry measurements, the anodic polarization started from the open-circuit voltage (OCV, i.e., the potential difference between the WE and RE under open-circuit conditions) to the 0.0 V (relative to the RE) at scan rate of 1 mV s^{-1}. It is important to note that the potential of the RE is the same as the CE (under open-circuit conditions) and therefore the potential difference between the WE and RE is taken as the OCV. In order to obtain an estimate of the power produced by the DCFC at a given current density, the anode potential (WE relative to RE) was multiplied by the corresponding current density to calculate the theoretical power density. In this work, there has been a focus on the maximum theoretical power density (P_{max}), i.e., the maximum value of the theoretical power density for a certain anode potential versus current density curve (or *V–i* curve). It should be pointed out that the real fuel cell power density is determined by the cell voltage (i.e., the potential difference between anode and cathode), and not just the anode potential. Since the reactivity of the anode was the main focus of this work, the cathode potential was not measured, and cell voltages are therefore not reported.

In the on-line measurements of anodic off-gas (evolved from the WE), the gas flow rate was measured by a soap film burette, and the gas compositions were analysed by gas chromatography (SHIMADZU GC-8A) with H_2 as the carrier gas. In the tests, the off-gas composition was initially analysed by gas chromatography with the current off to give a baseline, as well as with the current on to measure the gases produced by the electrochemical reaction. The current was controlled under potentiostatic conditions. Accordingly, the net electrochemical evolution rate of CO_2 (Q_{CO_2}) and total net electrochemical evolution rate of carbon oxides (CO_2 and CO) ($Q_{(CO_2+CO)}$) were calculated by the difference between the outlet flow rates with current on and the flow rates with current off, as expressed by [6]:

$$Q_{CO_2} = (X_{CO_2} Q_{Total})_{I-on} - (X_{CO_2} Q_{Total})_{I\text{-off}} \quad (6)$$

$$Q_{(CO_2+CO)} = [(X_{CO_2} + X_{CO}) Q_{Total}]_{I-on} - [(X_{CO_2} + X_{CO}) Q_{Total}]_{I\text{-off}} \quad (7)$$

where: X_{CO_2} and X_{CO} are the concentrations of CO_2 and CO in anodic off-gas determined by gas chromatography analysis; respectively; Q_{Total} is the total anodic off-gas evolution rate determined by bubble-meter measurement. Consequently, the yields of electrochemical CO_2 (Y_{CO_2}) and total electrochemical product gas (Y_{CO_2+CO}) can be calculated by [6]:

$$Y_{CO_2} = \frac{Q_{CO_2} F}{V_m I} \quad (8)$$

$$Y_{(CO_2+CO)} \frac{Q_{(CO_2+CO)} F}{V_m I} \quad (9)$$

where: F is the Faraday constant (96,485 C mol^{-1}); V_m (ml mol^{-1}) is the molar volume of CO_2 at standard temperature and pressure; I (A) is the current drawn from the DCFC during off-gas measurements.

The carbon efficiency (E_{Carbon}) is another useful parameter. It represents the ratio of electrochemical oxidation of carbon via an anodic reaction as per Eq. (1) to the total (chemical and electrochemical) carbon consumption, and can be calculated by [6]:

$$E_{Carbon} \frac{(1/3) Q_{CO_2}}{(1/2)(X_{CO} Q_{Total})_{I-on} + (1/3) Q_{CO_2}} \times 100\% \quad (10)$$

where the coefficients are determined by the molar ratios of the gas products to one mole of carbon reactant consumed in Eq. (1) and the Boudouard reaction Eq. (11) for CO_2 and CO, respectively.

$$CO_2(g) + C(s) = 2CO(g) \quad (11)$$

3. Results

3.1. Chemical analysis of coal samples

Table 1 compares the proximate analysis data (on the air-dried bases) of all coal samples obtained by TGA, i.e., the moisture, volatile matter, fixed carbon and ash contents. For all four raw coals, moisture accounts for less than 3 wt.% of the total weight, but there are obvious differences in the contents of volatile matter, fixed carbon and ash. GK is the highest ranked coal in these samples due to its highest fixed carbon (73.4 wt.%) and lowest volatile matter (19.6 wt.%) contents. By contrast, NL presents the lowest fixed carbon value (52.5 wt.%) and the highest ash content (16.7 wt.%) of all the coal samples. BW and KT show similar volatile matter and fixed carbon values, but the former has the highest volatile matter (32.7 wt.%) of all raw coals.

The mineral matter in coals is usually evaluated indirectly by analysing their ashes, which are transformed from mineral matter during coal combustion. Accordingly, the mineral matter of coals can be determined by analysing the elements in the ashes using a sensitive analytical technique such as inductively-coupled plasma optical emission spectrometry (ICPOES) [23,24]. Table 2 reports the compositions of the major and minor elements in the ashes of the

Table 1
Approximate analysis of coals by TGA.

Coal	Moisture (wt.%)	Volatile matter (wt.%)	Fixed carbon (wt.%)	Ash (wt.%)
BW	1.1	32.7	59.8	6.4
KT	2.5	31.3	61.7	4.5
NL	1.3	27.5	52.5	18.7
GK	1.2	19.6	73.4	5.8

Table 2
Ash composition of four raw coals.

Component	GK_{Ash} (wt.%)	BW_{Ash} (wt.%)	KT_{Ash} (wt.%)	NL_{Ash} (wt.%)
SiO_2	58.29	51.77	65.12	62.12
Al_2O_3	25.63	22.64	27.24	28.97
Fe_2O_3	3.89	9.79	3.43	2.58
TiO_2	1.71	0.96	1.41	2.15
CaO	2.32	5.86	0.05	0.04
MgO	0.27	1.41	0.08	0.02
Na_2O	0.85	1.01	0.47	0.22
K_2O	0.70	1.16	0.03	0.13
P_2O_5	1.94	2.83	0.08	0.34
Mn_3O_4	0.01	0.01	–	–
NiO	0.01	0.02	0.01	–
CuO	0.02	0.03	0.01	0.02
CoO	–	0.01	0.01	–
Cr_2O_3	0.01	0.01	0.01	0.01
Undetermined	3.35	2.49	2.05	3.40

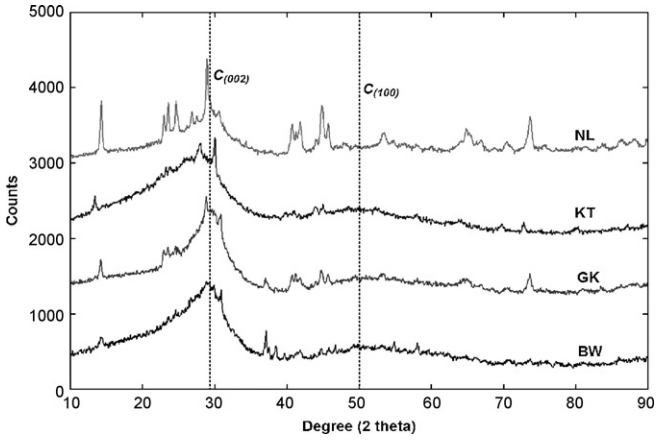

Fig. 2. XRD patterns of four raw coals.

four raw coals as determined by ICPOES; the elemental concentrations are given as oxides. The four ash samples are designated as GK_{Ash}, BW_{Ash}, KT_{Ash} and NL_{Ash}, respectively. The major minerals are SiO_2 and Al_2O_3 (70–90 wt.%), and the minor components are identified as Fe_2O_3, TiO_2, CaO, MgO, etc. The BW_{ash} sample, however, is different since it contains 9.79 wt.% Fe_2O_3 and more than 9 wt.% of alkali and alkaline earth metal oxides such as Na_2O, K_2O, MgO and CaO, which are at much higher levels than in the other three ashes. By contrast, the NL and KT ash samples are comprised of more than 90 wt.% of mineral matter in the form of SiO_2 and Al_2O_3, and less than 5 wt.% of mineral matter comprised Fe_2O_3, Na_2O, K_2O, MgO and CaO. It is also noticed that there are some undetermined elements (2.05–3.40 wt.%) in each ash sample, due to undetectable minor and trace elements in the ashes.

3.2. Graphitic structures of coal samples

The XRD patterns (with Co Kα radiation) of the four as-received coal samples are presented in Fig. 2. All samples contain a distinct (0 0 2) diffraction peak at around 29°, although it is extremely diffuse compared with that of ideal graphite. Another weak and broad (1 0 0) diffraction peak is present at around 50°. These peaks indicate that all coals contain a short-range graphite-like structure (or turbostratic structure) [25,26]. Certainly, there is also a significant amount of amorphous carbon in these coals, which contributes to the background intensity [26,27]. In addition to the carbonaceous diffraction peaks, the diffraction peaks corresponding to mineral inclusions are observed in these XRD patterns, especially for the NL sample in coincidence with its highest ash content (as shown in Table 1). The quantitative crystallite parameters of the four coal samples including the interplanar distance (d_{002}), the average diameter (La) and the stacking height (Lc) are also given in Table 3. The values of d_{002}, Lc and La vary in the narrow ranges of 0.354–0.365, 1.0–1.6 and 1.9–2.5 nm, respectively, and thereby indicate a similar disordered graphite structure in these four coals. The GK sample still shows the highest of graphite structure in these four coals, while the NL presents the lowest graphitic order.

Table 3
Crystalline parameters of coals.

Coal	XRD		
	d_{002} (nm)	Lc (nm)	La (nm)
BW	0.358	1.3	2.3
KT	0.365	1.1	2.2
NL	0.361	1.0	1.9
GK	0.354	1.6	2.5

3.3. Textural properties of coal samples

The textural properties and pore structures of coals have been shown to have important effects on the chemical and electrochemical reactions (oxidation and gasification) of carbon particles [28,29]. As a highly porous and heterogeneous solid, coal has a wide pore range from several nanometres to tenths of microns, which can be divided into micropores (with diameters less than 2 nm), mesopores (with diameters between 2 and 50 nm) and macropores (with diameters larger than 50 nm) [30,31]. Several techniques such as gas adsorption measurement, mercury porosimetry and microscopic analysis can be combined to give a better understanding of the textural properties of coals. In this work, the specific surface area, pore volume and average pore size of all coal samples are determined from the adsorption of N_2 at 77 K, and the microporous structures are characterized by CO_2 adsorption at 273 K.

The specific surface areas, pore volumes and average pore sizes of all coal samples are presented in Table 4. As expected, the specific surface area (S_{BET}) and pore volume (V_{total}) determined by N_2 adsorption are much smaller than the specific surface area (S_{micro}) and pore volume (V_{micro}) determined by CO_2. This difference has been well documented in the literature and is due to the microporous structure not being completely accessible to N_2 at 77 K because of an activated diffusion effect [32,33]. For the four as-received coals, GK shows the highest surface areas and pore volumes in both N_2 and CO_2 adsorption measurements, and thereby indicates the most developed porous nature of GK. The NL sample, however, presents the lowest S_{BET} and V_{total}, as well as the largest

Table 4
Textural properties of coals.

Coal	N_2 adsorption (77 K)			CO_2 adsorption (273 K)		
	S_{BET} ($m^2\ g^{-1}$)	V_{total} ($cm^3\ g^{-1}$)	D_{pore} (nm)	S_{micro} ($m^2\ g^{-1}$)	V_{micro} ($cm^3\ g^{-1}$)	D_{micro} (nm)
BW	4.6	0.009	3.20	134	0.058	1.26
KT	4.8	0.011	3.17	130	0.056	1.27
NL	3.3	0.005	3.27	99	0.046	1.30
GK	7.9	0.013	3.02	149	0.060	1.24

Table 5
Surface elemental compositions of coals by XPS.

Coal	C 1s (at.%)	O 1s (at.%)	N 1s (at.%)	S 2p (at.%)	Si 2p (at.%)	Al 2p (at.%)	(O/C) × 10^3	(N/C) × 10^3	(S/C) × 10^3	[(Si + Al)/C] × 10^3
BW	88.7	7.2	1.6	0.8	1.0	0.7	81.2	18.2	9.1	19.2
KT	87.5	7.4	2.1	1.6	0.8	0.6	85.4	24.1	18.3	16.0
NL	70.4	18.8	2.6	2.3	3.8	2.1	267.1	36.9	32.7	83.8
GK	86.8	9.1	1.3	0.6	1.5	0.7	105.7	15.0	6.9	22.3

pore size. This is probably due to the fact that it has the highest mineral content of all four raw coals, which is not accessible to N_2 molecules at low temperatures as emphasized above. The BW and KT samples have comparable textural properties, but the former shows a slightly higher surface area.

3.4. Surface functional groups on coal samples

The surface elemental compositions (by atomic concentration) of the all coals, as derived from their XPS survey spectra, are presented in Table 5. NL shows the lowest content of carbon on the surface, but the highest amounts of other elements such as oxygen, nitrogen, sulfur, silicon and aluminium. This observation is in agreement with the data given in Table 1 that show NL to have the lowest fixed carbon value, as well as the highest ash content. Consequently, the highest value of (O:C) in NL is mainly contributed by the inorganic oxygen contents, which originates from associated minerals such as SiO_2 and Al_2O_3 [34]. Although BW, KT and GK have a similar surface elemental content, GK shows a slightly higher value of (O:C) but lower values of both (N:C) and (S:C) than the other coals, due to the higher rank of GK that is consistent with previous reports [35,36].

Temperature-programmed desorption (TPD) is a popular technique for providing information about surface oxygen functional groups in coal samples, and Fig. 3(a) and (b) presents the TPD CO_2 and CO evolution profiles of the four raw coals, respectively. In the CO_2 evolution spectra, sample GK generates the most CO_2, with a broad peak at around 500 °C and a shoulder peak at around 700 °C. By contrast, NL presents the lowest evolution of CO_2 and shows a sharp peak at around 480 °C. Samples BW and KT have a comparable evolution of CO_2 with a maximum at around 450–500 °C, but the former coal produces slightly more CO_2. In the CO evolution curves, all the coals present a broad peak at around 550–850 °C, and the order of CO production is nearly the same as that of CO_2 production, namely, GK > BW > KT > NL.

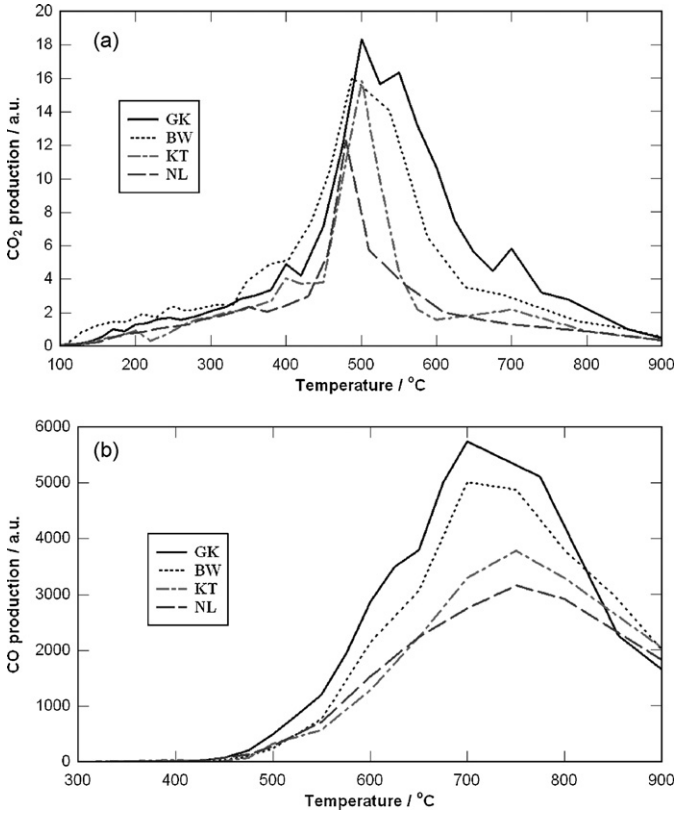

Fig. 3. TPD profiles of (a) CO_2 and (b) CO from four raw coals.

3.5. Electrochemical reactivity of coal samples in DCFC

3.5.1. Effect of coal types

Fig. 4 illustrates the anodic *V–i* curves of 5 wt.% GK, BW, KT and NL at 700 °C with 600 rpm stirring. Generally, the *V–i* curves of these coals are similar in shape. The curves all drop steeply from the OCV to around −0.8 V due to the activation resistance. Subsequently, a more stable linear region appears at a mid range of potentials (ca. from −0.8 to −0.4 V), which indicates that anodic polarization is under significant ohmic resistance control. Finally, the potential decreases sharply at high current density as fuel is consumed as fast as it is supplied to the electrode, i.e., the cell performance becomes mass-transport limited. The OCV, the current density (i) at a given potential and the theoretical peak power density (P_{Max}) of the coals at 600–800 °C are compared in Table 6. The GK sample shows the best overall electrochemical reactivity due to its most negative OCV, highest current density and P_{Max} at various temperatures. By contrast, the NL sample has the lowest electrochemical reactivity which is demonstrated by its lowest current density at a given potential, and the lowest P_{Max} of the four coals. Although BW and KT have comparable electrochemical reactivities at different temperatures, the former shows slightly better performance. Especially in the high anode potential region, BW shows the highest current density (see *i* at −0.9 V in Table 6), which indicates that it has the highest electrochemical activation rate. These results are consistent with the microstructure and surface properties of coal samples, which will be discussed in detail in Section 4.

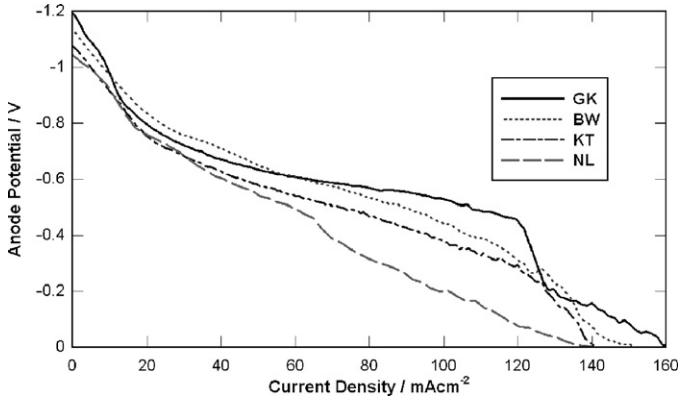

Fig. 4. Potential–density (or *V–i*) curves of 5 wt.% four raw coals at 700 °C and 600 rpm stirring.

Table 6
Electrochemical data of coals.

Operation conditions		BW	KT	NL	GK
600 °C, 600 rpm	OCV (V)	−1.02	−0.97	−0.94	−1.03
	i at −0.8 V (mA cm^{-2})	10	9	7	11
	i at −0.5 V (mA cm^{-2})	30	26	21	32
	i at −0.2 V (mA cm^{-2})	58	51	45	60
	P_{Max} (mW cm^{-2})	16	15	12	18
700 °C, 600 rpm	OCV (V)	−1.21	−1.11	−1.09	−1.19
	i at −0.9 V (mA cm^{-2})	14	10	9	11
	i at −0.6 V (mA cm^{-2})	59	49	41	60
	i at −0.3 V (mA cm^{-2})	128	117	82	122
	P_{Max} (mW cm^{-2})	45	39	30	53
800 °C, 600 rpm	OCV (V)	−1.32	−1.28	−1.25	−1.31
	i at −0.9 V (mA cm^{-2})	31	28	25	29
	i at −0.6 V (mA cm^{-2})	90	81	62	106
	i at −0.3 V (mA cm^{-2})	183	145	104	212
	P_{Max} (mW cm^{-2})	85	78	63	111

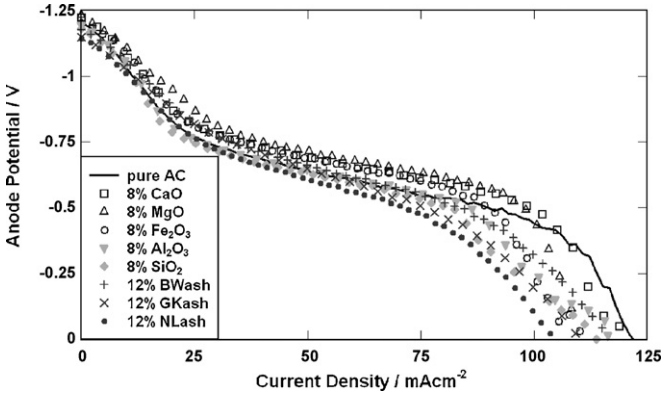

Fig. 5. Potential–density (or V–i) curves of 5 wt.% AC with different impurities at 700 °C and 600 rpm stirring.

3.5.2. Effect of mineral impurities

In the study of the effect of mineral impurities on the anodic reaction in the DCFC, a low-ash activated carbon (AC, with less than 1.5 wt.% ash) was selected as a standard carbon fuel. Each time, 12.5 g of AC was mixed with specific impurities such as 1 g CaO, 1 g MgO, 1 g Fe_2O_3, 1 g Al_2O_3, 1 g SiO_2, and 1.5 g coal ash of BW, NL and GK, respectively. Subsequently, the mixture of AC and impurity was added to the DCFC for electrochemical data collection as described in Section 2.2. The anodic V–i curves of pure AC before and after addition of various impurities are compared at 700 °C in Fig. 5. Although there is little difference between these curves, the presence of impurities can alternatively facilitate or impede the carbon anodic reaction in the DCFC. The minerals CaO, MgO and Fe_2O_3 have been found to be active catalysts for the anodic reaction, since the current densities at high anode potential (from OCV to −0.5 V, which are controlled by electrochemical activation) and P_{Max} all shift to higher values as shown in Table 7. By contrast, the current densities in the low anode potential region (from −0.5 to 0.0 V) do not show any improvement.

On the contrary, the V–i curves of Al_2O_3 and SiO_2 show a slight downwards shift that is probably due to the passivation or inhibitive effect of these oxides on the electrodes, as reported by others [6]. As a result, the P_{Max} of AC diminishes slightly after the addition of Al_2O_3 or SiO_2 to AC. In the study of the three coal ashes (BW_{Ash}, GK_{Ash} and NL_{Ash}) on the efficacy of the AC electrochemical reaction, there is almost no change in the current densities at high anode potential (see i at −0.9 V in Table 7). Whereas, the current densities at lower anode potential (see i at −0.3 V in Table 7) and P_{Max} obviously fall, which is a similar situation to that arising from the addition of Al_2O_3 and SiO_2 to AC. Interestingly, the OCV values increase by 30–60 mV when these coal ashes are added to the DCFC (see Table 7). As mentioned in Section 3.1, the main impurities in these coal ashes are Al_2O_3 and SiO_2. This further confirms that Al_2O_3 and SiO_2 may decrease the electrochemical performance of the DCFC probably due to their inhibitive effect on the electrodes. Interestingly, BW_{Ash} contains higher amounts of catalytic minerals such as Fe_2O_3, Na_2O, K_2O, MgO and CaO (see Table 2) than GK_{Ash} and NL_{Ash}. The addition of BW_{Ash} to AC results in the highest electrochemical reactivity, as illustrated by data in the final three rows of Table 7.

3.6. Anodic off-gas analysis

As shown in Figs. 6 and 7, both the electrochemical CO_2 yield (Y_{CO_2}) and the sum of CO_2 and CO yields ($Y_{(CO_2+CO)}$) of various coal samples are highly dependent on the operational temperature of the DCFC. From 600 to 700 °C, there are only slight increases in the Y_{CO_2} values within a range of 0.5–0.8. Similarly, the $Y_{(CO_2+CO)}$ values increase slightly from 600 to 700 °C and within a range of 0.6–0.8. These data are very close to the theoretical CO_2 evolution

Table 7
Electrochemical data of AC with different impurities at 700 °C with 600 rpm stirring.

Samples	OCV (V)	i at −0.9 V (mA cm^{-2})	i at −0.6 V (mA cm^{-2})	i at −0.3 V (mA cm^{-2})	P_{Max} (mW cm^{-2})
Pure AC	−1.21	16	62	112	46.3
8% CaO + AC	−1.22	18	80	110	50.9
8% MgO + AC	−1.22	22	85	103	51.8
8% Fe_2O_3 + AC	−1.20	17	74	97	47.3
8% Al_2O_3 + AC	−1.19	15	60	96	43.3
8% SiO_2 + AC	−1.18	14	56	92	40.8
12% BW_{Ash} + AC	−1.18	18	63	101	42.5
12% GK_{Ash} + AC	−1.16	16	57	94	38.2
12% NL_{Ash} + AC	−1.15	15	51	88	36.4

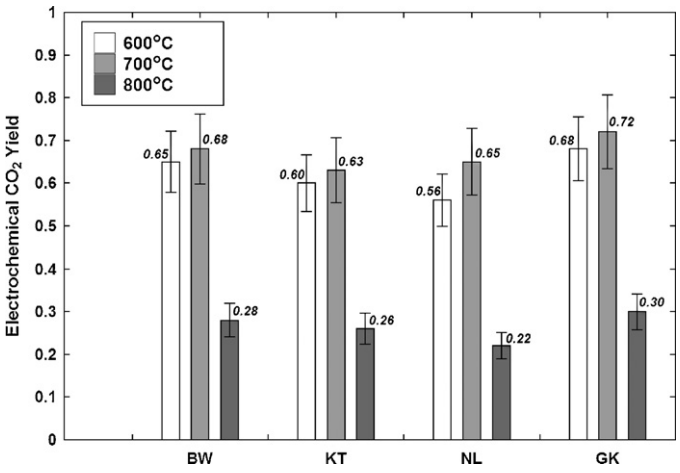

Fig. 6. Electrochemical CO_2 yield (Y_{CO_2}) of 5 wt.% coals at 600–800 °C.

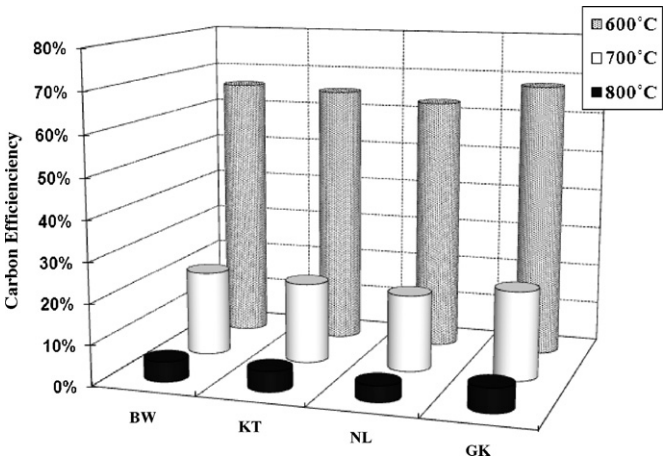

Fig. 8. Carbon efficiencies (E_{Carbon}) of 5 wt.% various coal samples at 600–800 °C with 600 rpm.

yield ($Y_{CO_2} = 0.75$) in the assumed main anodic reaction, as expressed by Eq. (1). This indicates that the main product for the electrochemical oxidation of carbon at 600–700 °C is CO_2 rather than CO. On the other hand, the Y_{CO_2} decreases to 0.2–0.35, and the $Y_{(CO_2+CO)}$ increases to 0.9–1.3 when the temperature rises to 800 °C. This may be caused by the Boudouard reaction, as expressed by Eq. (11), which can consume the electrochemical yield of CO_2 and solid carbon fuels at the WE at temperatures in excess of 700 °C [6,7]. Meanwhile, the electrochemical oxidation of coals at 800 °C may be explained by Eqs. (12) and (13), in which CO can be produced by electrochemical oxidation and the theoretical values of $Y_{(CO_2+CO)}$ are 1.0 and 1.5, respectively [7,37].

$$C + CO_3^{2-} = CO_2 + CO + 2e^- \quad (12)$$

$$2C + CO_3^{2-} = 3CO + 2e^- \quad (13)$$

The carbon efficiency (E_{Carbon}) of various coal samples at 600–800 °C, which can be calculated from Eq. (10), are compared in Fig. 8. With increase in temperature, the E_{Carbon} values decrease for all of the coals obviously due to the chemical loss of carbon by the Boudouard reaction at higher temperature. Especially at 800 °C, the E_{Carbon} values are less than 10% relative, which indicates that more than 90% relative of the carbon fuels are heavily consumed by the chemical Boudouard reaction. In the four raw coals, the highest E_{Carbon} value is found in GK at different temperatures, while the lowest carbon efficiency belongs to NL. It can be further stated that, of the four coals tested, GK is more accessible for electrochemical oxidation in the DCFC because it has the highest reactivity. The NL sample, however, yields a lower electrochemical reactivity than the other coals. These results are in good agreement with the electrochemical reactivities of different coal samples presented in Section 3.5.1.

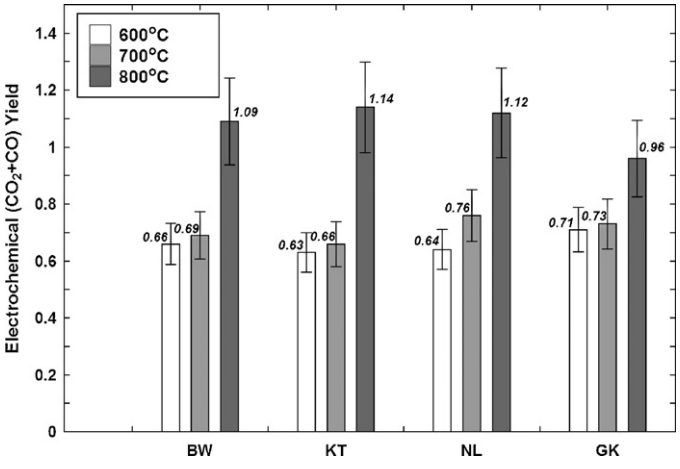

Fig. 7. Electrochemical CO_2 and CO yield ($Y_{(CO_2+CO)}$) of 5 wt.% coals at 600–800 °C.

4. Discussion

Based on the experimental results, the electrochemical reactivities of coals are highly dependent on their chemical and physical properties such as chemical composition, degree of graphitic character, surface areas and surface functional groups. For the four raw coals under examination, GK shows the highest overall electrochemical reactivity due to the following reasons: (1) it has the highest surface area and pore volume, as demonstrated by both N_2 and CO_2 adsorption measurements, which can improve the interaction between carbon fuels and the molten carbonate electrolyte; (2) GK is the highest ranked coal due to its highest fixed carbon (73.4 wt.%) and the lowest volatile matter (19.6 wt.%) content, as shown in Table 1, indicating that a higher carbon concentration in coal would be beneficial to its performance in a DCFC; (3) TPD showed GK to have the largest number of surface oxygen-containing functional groups, which is consistent with the reaction mechanism proposed by Cherepy et al. [2], i.e., oxygen surface functional groups provide more reactive sites and enhance the discharge rate of coals in a DCFC. As discussed previously [16,20–22], oxygen-containing surface functional groups are even more important than the surface area to the performance of a carbon in a DCFC. In contrast to GK, NL has the lowest electrochemical reactivity of the four coals, which is attributed to its low surface area and pore volume, small amount of surface oxygen-containing functional groups, low fixed carbon concentration, and high ash content. Although the BW and KT coals have similar chemical compositions and textural properties, TPD shows that the former has more surface oxygen-containing functional groups than the latter, which results in a different electrochemical reactivity in a DCFC. Nevertheless, the differences in crystalline structure of the four coals are almost negligible, and cannot be correlated with their electrochemical reactivities.

Levels of metal oxides similar to those found in the coals have been added to activated carbon (see Table 7), so as to investigate the influence of mineral impurities on the anodic electrochemical reactivity of a DCFC and, since some of these metals (Li, Na, K, Ca, Mg, Fe, Cu, Cr, Co, Ni, etc.) and their oxides exhibit catalytic effects, on various chemical reactions with coals such as gasification, hydrogenation and oxidation [23,38]. In this study, it is assumed that the basic mechanism of coal oxidation in a DCFC is similar to the chem-

ical oxidation of coals suggested by others [6]. As shown in Section 3.5.2, the addition of CaO, MgO and Fe_2O_3 into the melt slightly increases the current density in a high anode potential region (controlled by electrochemical activation), which indicates that the three mineral impurities might have a catalytic effect on the anodic oxidation of the carbon fuel. A decrease in anodic electrochemical reactivity of pure AC, however, is observed after introducing Al_2O_3 and SiO_2 impurities into the electrolyte. Meanwhile, the addition of coal ash to the AC obviously decreases the current density in the low anode potential region, indicating a decrease in the mass transfer at the electrodes. This further confirms the inhibitive effect of Al_2O_3 and SiO_2 on the electrodes as they are the major impurities in coal ashes (see Table 2). In fact, there are various amounts of catalytic impurities such as alkali and alkaline earth metal oxides in the three coal ashes, as shown in Table 2. It must be noted that the catalytic activity of mineral inclusions is highly dependent on their concentration, dispersion, chemical form and stability in the coal matrix [23]. In this study, less than 10 wt.% of the coal ashes had potential catalytic impurities and the chemical forms of these mineral impurities may be transformed during high-temperature operation and thereby result in a comparable lower catalytic effect of the coal ashes on the electrochemical oxidation of AC.

5. Conclusions

The feasibility of coals as fuels in the DCFC has been confirmed by electrochemical data obtained for four raw coals. An important outcome is the observation that the complete oxidation of carbon (in coal) to CO_2 can be achieved at 600–700 °C, while carbon is only partially oxidised electrochemically into CO at 800 °C. The fixed carbon concentration, surface area, surface oxygen functional groups and composition of minerals are important factors in determining the electrochemical performance of a DCFC. During studies of the effect of mineral impurities on the electrochemical reaction in a DCFC, Al_2O_3 and SiO_2 are found to exhibit an inhibitive effect on the anodic reaction, while CaO, MgO and Fe_2O_3 display a catalytic effect on the electrochemical oxidation of carbon. Consequently, it is highly recommended that appropriate pre-treatment of coals (such as demineralization of the inhibitive impurities) should be employed to produce desirable carbon fuels for DCFCs.

Acknowledgement

Financial support from the ARC (Australian Research Council) Discovery project is greatly appreciated.

References

[1] I.E. Agency, World Energy Outlook 2007 China and India Insights, IEA, Paris, 2007, p. 663.
[2] N.J. Cherepy, R. Krueger, K.J. Fiet, A.F. Jankowski, J.F. Cooper, J. Electrochem. Soc. 152 (2005) A80.
[3] D. Cao, Y. Sun, G. Wang, J. Power Sources 167 (2007) 250.
[4] M.J. Antal, G.C. Nihous, Ind. Eng. Chem. Res. 47 (2008) 2442.
[5] S. Zecevic, E.M. Patton, P. Parhami, Carbon 42 (2004) 1983.
[6] D.G. Vutetakis, D.R. Skidmore, H.J. Byker, J. Electrochem. Soc. 134 (1987) 3027.
[7] R.D. Weaver, L. Nanis, J. Electrochem. Soc. 127 (1980) C410.
[8] G.A. Hackett, J.W. Zondlo, R. Svensson, J. Power Sources 168 (2007) 111.
[9] T. Nunoura, K. Dowaki, C. Fushimi, S. Allen, E. Meszaros, M.J. Antal, Ind. Eng. Chem. Res. 46 (2007) 734.
[10] T.M. Gur, R.A. Huggins, J. Electrochem. Soc. 139 (1992) L95.
[11] K. Pointon, B. Lakeman, J. Irvine, J. Bradley, S. Jain, J. Power Sources 162 (2006) 750.
[12] A.C. Lee, S. Li, R.E. Mitchell, T.M. Gur, Electrochem. Solid-State Lett. 11 (2008) B20.
[13] M. Ihara, S. Hasegawa, J. Electrochem. Soc. 153 (2006) A1544.
[14] B.G. Miller, Coal Energy Systems, Elsevier Academic Press, Boston, Mass, 2005, p. 526.
[15] A.L. Dicks, J. Power Sources 156 (2006) 128.
[16] X. Li, Z.H. Zhu, R. De Marco, J. Bradley, A. Dicks, J. Phys. Chem. A, in press.
[17] M.C. Mayoral, M.T. Izquierdo, J.M. Andres, B. Rubio, Thermochim. Acta 370 (2001) 91.
[18] L.R. Radovic, P.L. Walker Jr., R.G. Jenkins, Fuel 62 (1983) 849.
[19] Z.H. Zhu, L.R. Radovic, G.Q. Lu, Carbon 38 (2000) 451.
[20] X. Li, Z. Zhu, J. Chen, R. De Marco, A. Dicks, J. Bradley, G. Lu, J. Power Sources 186 (2009) 1.
[21] X. Li, Z.H. Zhu, R. De Marco, A. Dicks, J. Bradley, S. Liu, G.Q. Lu, Ind. Eng. Chem. Res. 47 (2008) 9670.
[22] X. Li, Z.H. Zhu, R. De Marco, A. Dicks, J. Bradley, Energy Fuels 23 (2009) 3721.
[23] J.G. Speight, The Chemistry and Technology of Coal, M. Dekker, New York, 1994, p. 642.
[24] R. Gupta, Energy Fuels 21 (2007) 451.
[25] L. Lu, C. Kong, V. Sahajwalla, D. Harris, Fuel 81 (2002) 1215.
[26] L. Lu, V. Sahajwalla, C. Kong, D. Harris, Carbon 39 (2001) 1821.
[27] Q. Lin, J.M. Guet, Fuel 69 (1990) 821.
[28] P.L. Walker, S.K. Verma, J. Rivera-Utrilla, A. Davis, Fuel 67 (1988) 1615.
[29] T. Kabe, A. Ishihara, E.W. Qian, I.P. Sutrisna, Y. Kabe, Stud. Surf. Sci. Catal. (2004) 150.
[30] J. Yu, J.A. Lucas, T.F. Wall, Prog. Energy Combust. Sci. 33 (2007) 135.
[31] S.J. Gregg, K.S.W. Sing, Adsorption, Surface Area, and Porosity, Academic Press, London, 1982, p. 303.
[32] I.G. Senel, A. Guruz, H. Yucel, Energy Fuels 15 (2001) 331.
[33] D. Cazorla-Amoros, J. Alcaniz-Monge, M.A. de la Casa-Lillo, A. Linares-Solano, Langmuir 14 (1998) 4589.
[34] G. Domazetis, M. Raoarun, B.D. James, J. Liesegang, P.J. Pigram, N. Brack, R. Glaisher, Energy Fuels 20 (2006) 1556.
[35] S.R. Kelemen, M. Afeworki, M.L. Gorbaty, A.D. Cohen, Energy Fuels 16 (2002) 1450.
[36] R. Pietrzak, T. Grzybek, H. Wachowska, Fuel 86 (2007) 2616.
[37] K. Sasaki, A. Kunai, T. Sada, Denki Kagaku 48 (1980) 311.
[38] D.W.v. Krevelen, Coal: Typology, Physics, Chemistry, Constitution, Elsevier Science, Amsterdam, 1993, p. 979.